


## Article

# Mechanical and Freeze-Thaw Characterization of Lignin-BFS (GGBS)-Modified Silty Clays

Yidan Sun <sup>1,\*</sup>, Fujun Yu <sup>1</sup>, Yu Yang <sup>2,3</sup>, Chao Li <sup>1</sup>, Songling Xue <sup>1</sup> and Jiankun Huang <sup>1</sup>

<sup>1</sup> School of Civil and Ocean Engineering, Jiangsu Ocean University, Lianyungang 222000, China; yufujun202202@163.com (F.Y.); gbyghb67@163.com (C.L.); xuezhiying@my.swjtu.edu.cn (S.X.); pubum329@163.com (J.H.)

<sup>2</sup> School of Civil Engineering, Liaoning Technical University, Fuxin 123000, China; yangyu9300@163.com

<sup>3</sup> School of Safety Science and Engineering, Xinjiang Institute of Engineering, Urumchi 830023, China

\* Correspondence: 2020000083@jou.edu.cn

**Abstract:** Using silty clay as roadbed filling can lead to roadbed diseases. In this paper, silty clay was modified with lignin and BFS (GGBS). Then, the mechanical properties, freeze-thaw characteristics, and microscopic mechanisms were investigated using unconfined compression tests, California bearing ratio tests, rebound modulus tests, freeze-thaw cycling tests, scanning electron microscopy (SEM), and X-ray diffraction (XRD). The results showed that as the curing age increased, the unconfined compressive strength (UCS) of modified silty clay gradually increased, and the relationship between the stress and axial strain of the samples gradually transitioned from strain-softening to strain-hardening. As the lignin content decreased and the BFS content increased, the UCS, California bearing ratio (CBR), and rebound modulus of the modified silty clay first increased and then tended to stabilize. Adding lignin and BFS can effectively resist volume increase and mass loss during freeze-thaw cycles. When the ratio of lignin to BFS was 4%:8%, the growth rate of the UCS, CBR, and rebound modulus was the largest, the change rate in volume and mass and the loss rate of the UCS under the freeze-thaw cycle were the smallest, and the silty clay improvement effect was the most significant. The microscopic experimental results indicated that a large amount of hydrated calcium silicate products effectively increased the strength of interunit connections, filled soil pores, and reduced pore number and size. The research results can further improve the applicability of silty clay in roadbed engineering, protect the environment, and reduce the waste of resources.

**Keywords:** lignin; BFS; mechanical properties; freeze-thaw properties; microscopic mechanisms



Academic Editors: Mijia Yang and Mohamed K. Ismail

Received: 24 October 2024

Revised: 10 December 2024

Accepted: 24 December 2024

Published: 26 December 2024

**Citation:** Sun, Y.; Yu, F.; Yang, Y.; Li, C.; Xue, S.; Huang, J. Mechanical and Freeze-Thaw Characterization of Lignin-BFS (GGBS)-Modified Silty Clays. *Buildings* **2025**, *15*, 38. <https://doi.org/10.3390/buildings15010038>

**Copyright:** © 2024 by the authors. Licensee MDPI, Basel, Switzerland. This article is an open access article distributed under the terms and conditions of the Creative Commons Attribution (CC BY) license (<https://creativecommons.org/licenses/by/4.0/>).

## 1. Introduction

A large amount of silty clay is widely distributed in the Lianyungang area, characterized by high natural water content, high compressibility, and low strength. Using them directly as roadbed fillers can lead to problems such as slope collapse, collapse, and roadbed subsidence, which poses huge challenges to design and construction and even causes certain economic losses [1–4]. Addressing the performance of poor roadbed soil has been a research focus, and geosynthetic reinforcement and chemical improvement are commonly used in engineering [5–7]. Traditional modifiers, such as lime and cement [8,9], have been proven to be effective materials for improving the performance of subgrade soil, but the dust, carbon dioxide, sewage, and residues generated during their production pose hazards to ecosystems and human health [10,11]. Therefore, there is an urgent need to find other more environmentally friendly alternatives. Industrial waste, as a sustainable and

environmentally friendly alternative to cementitious materials, can reduce the high cost and environmental problems caused by traditional modifiers [12–14].

Lignin and BFS (BFS) are considered modifiers that can improve soil performance and add no pollution into the ecological environment, although they are not reasonably utilized. Some scholars have carried out research regarding adding lignin and BFS into the soil [15–21]. Lignin, composed of various hydroxyl and aromatic groups, is often used in pavement asphalt modification [15]. A large number of mechanical experiments have shown that the addition of lignin can significantly improve the shear strength and UCS of soil, but excessive or insufficient lignin content is not conducive to further growth of soil strength [22–24]. Additionally, lignin can inhibit soil disintegration and improve soil water stability through particle aggregation. The adsorption of lignin causes soil particles to agglomerate and restricts water entry into the soil, which explains why lignin-treated soil after the freeze-thaw cycle shows fewer cracks and pores than undisturbed soil [25–29]. BFS has a wider range of applications in modified soils compared to lignin. BFS, an industrial by-product, can generate hydration products through volcanic ash reactions and is often used as a cementitious material [30]. A large number of mechanical and microscopic tests have shown that BFS can significantly improve the mechanical characteristics of the soil because reaction products, such as C-(A)-S-H gels, enhance the bonding between soil particles and fill in the microscopic pores [31–36]. The active ingredients in BFS can act synergistically with other industrial wastes, e.g., fly ash (FA), resulting in a superior modification effect compared to single-mixed BFS [37,38]. In addition, under dry-wet and freeze-thaw cycles, BFS can significantly improve the mechanical properties of frozen soil [39,40]. However, the early strength of BFS-treated soil increases slowly without alkali excitation, and the strength effects of different alkaline chemical admixtures are also different [41–44].

In summary, lignin and BFS, as environmentally friendly industrial wastes, are widely used in soil modification. At present, there is relatively little research on the mechanical properties and freeze-thaw characteristics of lignin composite BFS-modified silty clay. This paper studied the effects of lignin and BFS on the mechanical properties and freeze-thaw characteristics of silty clay through unconfined compression tests, California bearing ratio tests, rebound modulus tests, and freeze-thaw cycle tests. Then, correlation analysis was used to determine the optimal dosage of lignin and BFS. Finally, combining XRD and SEM experiments, the intrinsic mechanism of lignin-BFS-modified silty clay was revealed.

## 2. Test Program

### 2.1. Test Materials

The silty clay, lignin, and BFS (Figure 1) used in the test were all taken from Lianyungang City, Jiangsu Province, China; the basic physical indicators are shown in Tables 1 and 2. Lignin was obtained from a byproduct of a local biomass processing enterprise in Lianyungang. The lignin waste generated during the production process of the enterprise was collected and initially treated for this experimental study, aiming to explore its application potential in improving the performance of silty clay and realize the resource utilization of waste. Lignin is a brownish-yellow powder with a special aromatic odor. It is a polymer anionic surfactant with strong dispersibility, adhesion, and coordination. It mainly contains active functional groups, e.g., alcohol hydroxyl groups ( $-OH$ ,  $3374\text{ cm}^{-1}$ ), benzene ring  $C=C$  bonds ( $651$ ,  $880$ ,  $1593\text{ cm}^{-1}$ ), alkanes ( $C-H(CH_2)$ ,  $1423$ , and  $1593\text{ cm}^{-1}$ ), primary alcohols ( $R_1-CH_2-OH$ ,  $1050\text{ cm}^{-1}$ ), and secondary alcohols ( $R_1-CH(R_2)-OH$ ,  $1090\text{ cm}^{-1}$ ) [45]. The relative density of lignin is usually between 1.35–1.50, it is optically inactive and has a refractive index, is soluble in water, and has most common organic solvents in its natural form. The viscosity of lignin solutions is generally low, has thermoelectricity, and the softening temperature is usually between 120–200 °C. When lignin contains water, its glass

transition temperature ( $T_g$ ) is significantly reduced. As a polymer anionic surfactant, lignin can change the particle distribution, enhance the soil deformation resistance, and create good conditions for the subsequent reaction. By forming covalent bonds with clay minerals and promoting the BFS hydration reaction, the soil strength is enhanced to better withstand external pressure. In terms of water stability, it regulates water distribution and migration, stabilizes the aggregate structure, reduces expansion and dispersion when it meets water, and performs well in the freeze-thaw cycle.



Figure 1. Test materials.

Table 1. Basic physical properties of the silty clays used in the tests.

Density $/(g \cdot cm^{-3})$	Water Content/%	Liquid Limit/%	Plastic Limit/%	Plasticity Index	Relative Density	Maximum Dry Density $/(g \cdot cm^{-3})$	Optimum Water Content/%
1.44	43.41	41.18	19.86	21.32	2.7	1.61	20.63

Table 2. Basic physical properties of GGBS used in the test.

Specific Surface Area ( $m^2/kg$ )	Turnover Ratio (%)	Density $(g/cm^3)$	Heat Loss (%)	CaO (%)	SiO <sub>2</sub> (%)	Al <sub>2</sub> O <sub>3</sub> (%)	SO <sub>3</sub> (%)	Fe <sub>2</sub> O <sub>3</sub> (%)	MgO (%)
429.00	98.00	3.10	0.84	34.00	34.50	17.70	1.64	1.03	6.01

## 2.2. Experimental Design and Experimental Methods

Based on Zhang Jianwei's research results and preliminary experimental results [46], the optimum dosage of modifiers is 12%, and the mix design is shown in Table 3.

Table 3. Design of mixing proportions.

Sample No.	The Proportion of Silt Soil (%)	Lignin: GGBS	Optimum Moisture Content (%)	Maximum Dry Density ( $g/cm^3$ )	Curing Age
S1	100%	0	20.63	1.59	7D, 14D, 28D
S2	88%	12%:0%	21.98	1.65	7D, 14D, 28D
S3	88%	8%:4%	21.78	1.64	7D, 14D, 28D
S4	88%	4%:8%	19.73	1.62	7D, 14D, 28D
S5	88%	0%:12%	19.1	1.61	7D, 14D, 28D

Compaction preparation: The silty clay, lignin, and blaster slag (BFS) raw materials were proportionally weighed and placed in a mixing container to form a homogeneous mixture through mechanical agitation. The mixture was transferred to the corresponding mold and then pressed with a press to keep the pressure stable. The pressure time was a few minutes to tens of minutes, and then the molding sample was removed. The sample had high density, a stable structure, a compact particle arrangement, and small porosity.

The unconfined compressive strength test can simulate the stress state and reflect the compressive performance. The deformation and bearing capacity can be reflected in the CBR test. The freeze-thaw cycle test can effectively reflect the stability of engineering applications in cold areas.

Unconfined compressive strength test (UCS test): the samples ( $\varphi 50 \text{ mm} \times h 50 \text{ mm}$ ) were measured at 7, 14, and 28 d for compressive strength following Chinese standard JTG 3430-2020 [47]. A hydraulic universal testing machine with a displacement control loading at 1 mm/min was employed.

CBR test and rebound modulus test: the samples ( $\varphi 152 \text{ mm} \times h 170 \text{ mm}$ ) were measured at 7, 14, and 28 d for CBR and rebound modulus following Chinese standard JTG 3430-2020 [47]. The CBR and rebound modulus were measured with a strength meter, and the loading rate was 1 mm/min.

Freeze-thaw cycle test: the samples at a curing age of 28 d were selected for the freeze-thaw cycle test. Each freeze-thaw cycle was 24 h, containing a 12 h freezing phase and a 12 h melting phase. The temperature of the freeze-thaw test was based on the meteorological data of Lianyungang City, Jiangsu Province, with a freezing temperature of  $-12 \text{ }^{\circ}\text{C}$  and a melting temperature of  $12 \text{ }^{\circ}\text{C}$ . The number of freeze-thaw cycles was set to 0, 1, 3, 5, and 10. The vernier caliper and electronic balance were used to measure the volume and mass change after the freeze-thaw cycle.

SEM and XRD tests: To investigate the mineralogical composition and analyze the microstructure, SEM and XRD tests were conducted on both improved and unprocessed soil samples after freeze-thaw cycles of 0, 5, and 10 times. Representative fragments from the UCS-tested samples were placed in the oven at  $50 \text{ }^{\circ}\text{C}$  for drying. Dry samples were tested after gold spraying using a TESCAN-VEGA3 scanning electron microscope [39]. For XRD analysis, both improved and unprocessed soil samples were examined using an X-ray diffractometer model Rich-Siefert equipped with a nickel filter. The scan was conducted with a rate of  $2\theta$  ranging from 0 to  $100^{\circ}/\text{s}$ , using increments of 0.5 degrees per second.

The sample preparation process and the test instruments are shown in Figure 2.

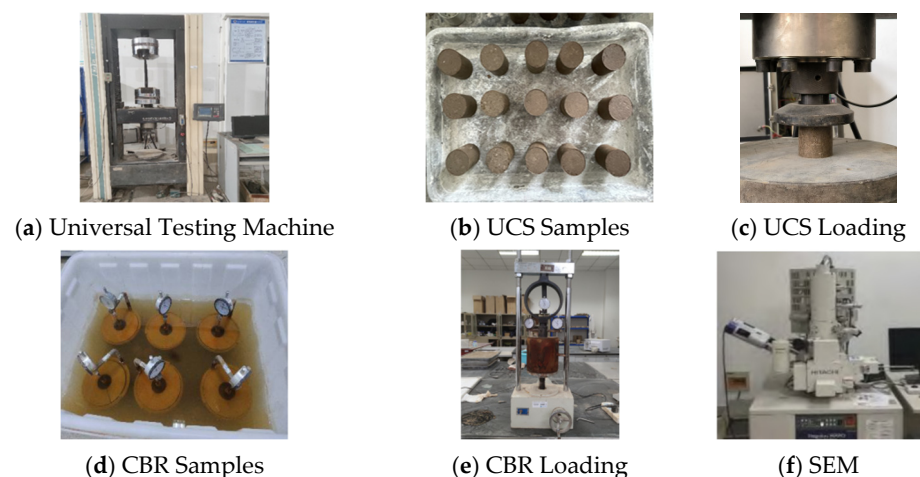


**Figure 2.** The sample preparation process and the test instruments.

### 3. Test Results and Analysis

#### 3.1. Analysis of Curing Unconfined Compressive Strength

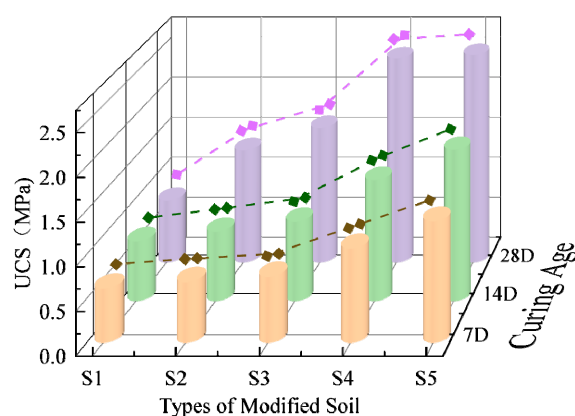
Characteristics of the Strain-Softening Curve: In the strain-softening stage, as the axial strain increases, the stress first reaches a peak value, and then, with the further increase in strain, the stress begins to gradually decrease. This means that after reaching the maximum bearing capacity, the material's ability to resist deformation gradually weakens, showing a



gradually softening characteristic. For example, in the silty clay without or with a small amount of additives (such as the S1 sample in the early stage), this situation may occur, and its stress-strain curve shows a relatively rapid decrease in stress after reaching the peak stress.

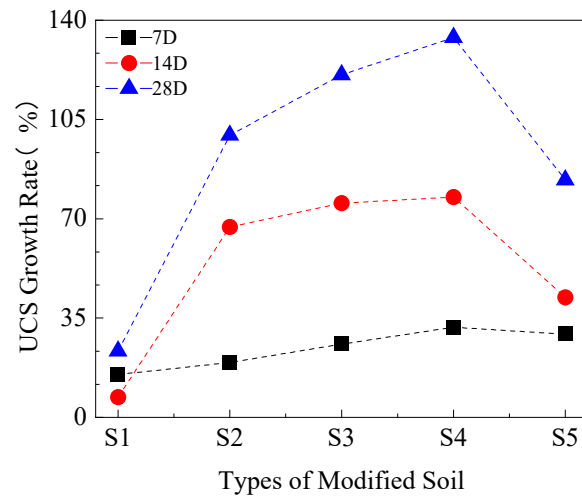
**Characteristics of the Strain-Hardening Curve:** Strain-hardening is different. As the axial strain increases, the stress continues to increase, and the material shows an increasingly stronger ability to resist deformation and becomes harder. When the lignin content decreases and the BFS (GGBS) content increases (such as in the S2–S5 samples with the increase in curing age and the effect of the additives), the stress-strain curve gradually shows the characteristic of strain-hardening, that is, the peak stress continuously increases, and after reaching the peak stress, the stress decrease trend slows down or remains relatively stable, indicating that the improved silty clay can still maintain a relatively high bearing capacity when subjected to larger deformation.

Figure 3 shows the UCS of the samples at different curing ages. At the same curing age, the addition of lignin-BFS significantly improves the UCS of silty clay. With the decrease in lignin content and the increase in BFS content, the UCS increases first and then becomes stable. After 28 d of curing, the UCS of the S2–S5 samples increased by 1.8 times, 2.18 times, 3.31 times, and 3.36 times, respectively, compared to the S1 samples. In the curing process, lignin locks water by attracting clay particles to form aggregates and promotes the formation of BFS hydration products, thus filling the internal pores of the soil and improving the strength of the soil.



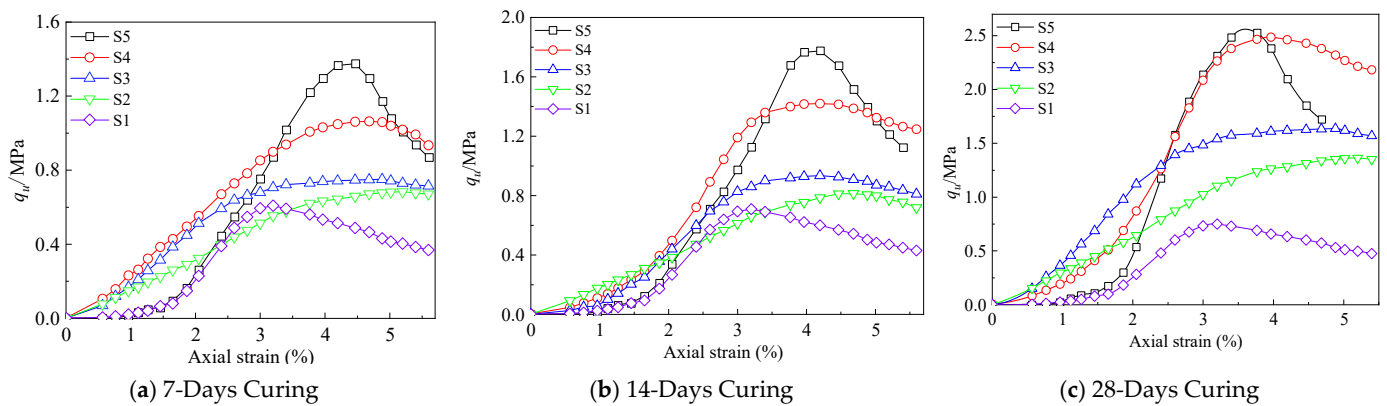
**Figure 3.** Three-dimensional diagram of UCS.

Figure 4 shows the variation of the UCS growth rate of the sample. At the same curing age, with the decrease in lignin content and the increase in BFS content, the UCS growth rate increases first and then decreases, indicating that there is an optimal amount of lignin and BFS. Among the five groups of the samples, the UCS growth rate of the S4 samples is the highest, which indicates that the content of lignin and BFS in the S4 samples is the best. Excessive lignin content will occupy the position of soil particles, leading to incomplete hydration reactions. Insufficient lignin will prolong the hydration reaction cycle of BFS, resulting in insignificant growth of the UCS. Moreover, the larger the proportion of BFS, the more the active components in BFS cannot fully hydrate, which has little effect on the strength growth of soil. Therefore, there is a balance point between lignin and BFS content. In addition, the reaction between the modifier and silt clay is most rapid from 14 d to 28 d. The reason for this is that the strength of BFS increases slowly without the action of strong alkaline activators [41]. With the increase in curing time, the internal hydration products increase, resulting in a higher rate of soil strength growth.



**Figure 4.** The growth rate of UCS.

Figure 5 shows the stress-strain curves at different curing ages. At the same curing age, the peak stress of the S2–S5 samples is significantly higher than that of the S1 sample. There are significant differences in the stress-strain curves of the S2–S5 samples. As the lignin content decreases and the BFS content increases, the stress-strain curves of S2–S5 transition from strain-softening to strain-hardening. At the same curing age, the peak stress of the unmodified S1 sample was significantly higher than that of the lignin-GGBS-modified S2–S5 sample. At the same time, the stress-strain curves of S2–S5 samples showed significant differences. With the decrease in lignin content and the increase in GGBS content, the curves showed a change from strain-softening to strain-hardening. During the 7-day curing period, each curve shape initially showed this trend (as shown in Figure 5a).



**Figure 5.** Stress-strain curves at different curing ages.

With the increase in curing age, the peak stress of the same group of samples increases significantly, the strain rate accelerates, and the peak strain shows a trend of moving forward, indicating that the transition from the plasticity to brittleness of the samples is more significant, which is similar to the properties of the most modified soils [48]. The reason for this is that during the long-term curing process, the hydration inside the samples continues to occur, leading to an increase in the brittleness of the samples. At the same curing age, the stress-strain curve of the S4 sample covers a larger area, indicating that the samples have better deformation resistance and plasticity after cracking [32], and the residual strength is correspondingly increased. Therefore, the dosage of lignin and BFS in S4 is the most suitable.

### 3.2. Analysis of CBR and Modulus of Resilience

From Figures 6–8, it can be seen that the addition of lignin-BFS significantly improves the CBR and rebound modulus of silty clay. As lignin content decreases and BFS content increases, the CBR and rebound modulus first increase and then flatten, and the CBR growth rate first increases and then decreases at the same curing age, which is roughly the same as the law of the UCS. There is a certain correlation between CBR and UCS [49]. After 28 d of curing, the CBR of the S1~S5 samples is 6.42%, 16.64%, 34.67%, 42.95%, and 44.28%, respectively. The CBR and rebound modulus of S2~S5 meet the requirements of subgrade filler for expressways in the Chinese standard JTG D50-2017; S1 samples do not meet the requirements [50]. The CBR growth rate of S4 was the highest (60.56%), indicating that the ratio of lignin and BFS in the S4 sample was the best. During the 14- to 28-day curing period, the rebound modulus of S4 increased the fastest, increasing by 63.94 MPa. The total increase in the rebound modulus of S2 and S5 was close to the increase in S4, indicating that the effect of composite improvers on improving soil is better than that of single improvers.

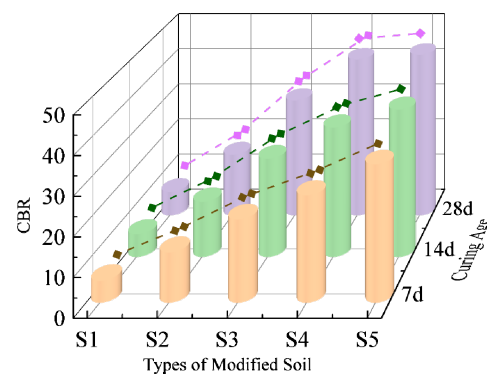


Figure 6. CBR at different curing ages.

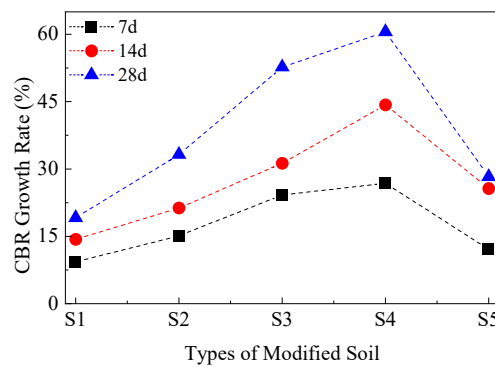


Figure 7. CBR growth rate at different curing ages.

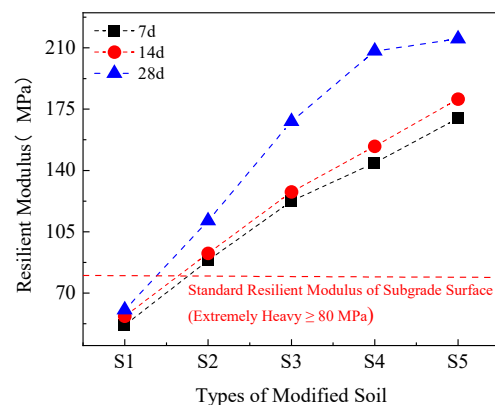


Figure 8. Rebound modulus at different curing ages.

### 3.3. Freeze-Thaw Cycles

The volume change rate and mass change rate are used to describe the volume and mass change of the samples during the freeze-thaw process, and the formulas are as follows:

$$\Delta V = \frac{V_a - V}{V} \times 100\% \quad (1)$$

$$\Delta m = \frac{m_a - m}{m} \times 100\% \quad (2)$$

where,  $\Delta V$  and  $\Delta m$  are the rate of volume and mass change, respectively;  $V_a$  and  $m_a$  are the volume and mass of the sample after each freezing/thawing, respectively;  $V$  and  $m$  are the initial volume and mass of the sample, respectively.

From Figure 9, it can be seen that during a single freeze-thaw cycle, both the volume and mass of the samples show a trend of first decreasing and then increasing, exhibiting a phenomenon of freeze-shrinkage and thawing expansion [51]. In general, with the increase in freeze-thaw times, the volume of the sample showed an increasing trend, while the mass showed a decreasing trend.

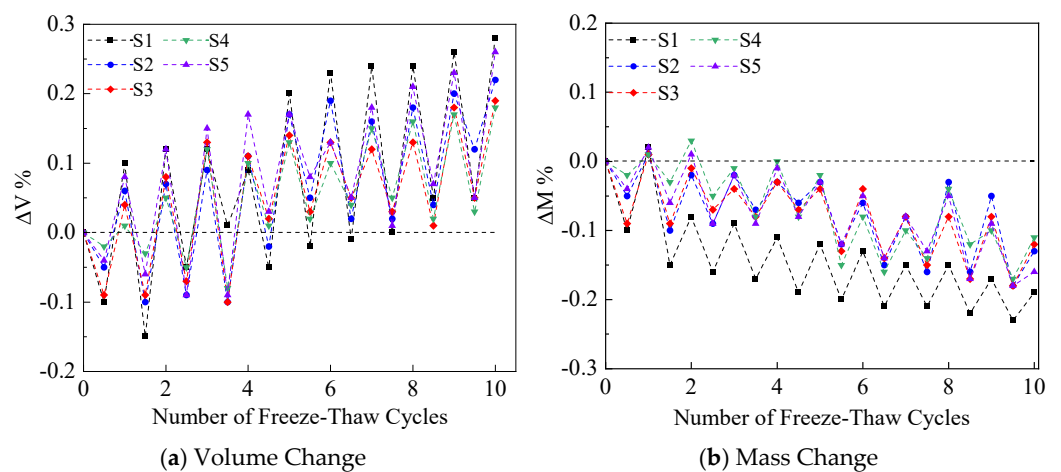


Figure 9. Mass and volume changes.

As shown in Table 4, after 10 freeze-thaw cycles, the volume change rates of the S1~S5 samples were 0.28%, 0.22%, 0.19%, 0.18%, and 0.26%, respectively, and the mass change rates were  $-0.19\%$ ,  $-0.13\%$ ,  $-0.12\%$ ,  $-0.11\%$ , and  $-0.16\%$ , respectively. The volume and mass changes of the S2~S5 samples were significantly lower than those of the S1 sample, indicating that the addition of lignin and BFS can effectively resist freeze-thaw effects. Among the five groups, the S4 sample has the smallest volume and mass changes; therefore, the dosage ratio of S4 is optimal.

Table 4. Mass and volume change rates under freeze-thaw cycles.

Number of Freeze-Thaw Cycles (Time)	Volume Change Rate (%)					Mass Change Rate (%)				
	S1	S2	S3	S4	S5	S1	S2	S3	S4	S5
1	0.1	0.06	0.04	0.01	0.08	0.02	0.01	0.01	0.01	0.02
3	0.12	0.07	0.08	0.05	0.12	$-0.09$	$-0.02$	$-0.04$	$-0.01$	$-0.02$
5	0.2	0.17	0.14	0.13	0.17	$-0.09$	$-0.03$	$-0.04$	$-0.02$	$-0.03$
10	0.28	0.22	0.19	0.18	0.26	$-0.20$	$-0.13$	$-0.12$	$-0.11$	$-0.16$

Figure 10 shows the apparent changes of the S1 sample and the S4 sample during the freeze-thaw cycle. With the increase in freeze-thaw times, soil particles fell off, and cracks occurred on the surface of the S1 sample first, and then surface cracks gradually expanded. After 10 freeze-thaw cycles, the cracks inside the samples were connected, and the soil particles on the surface significantly fell off. However, during the freeze-thaw cycle, the surface of the S4 sample had no obvious soil particle shedding and cracks, showing significant freeze-thaw resistance.

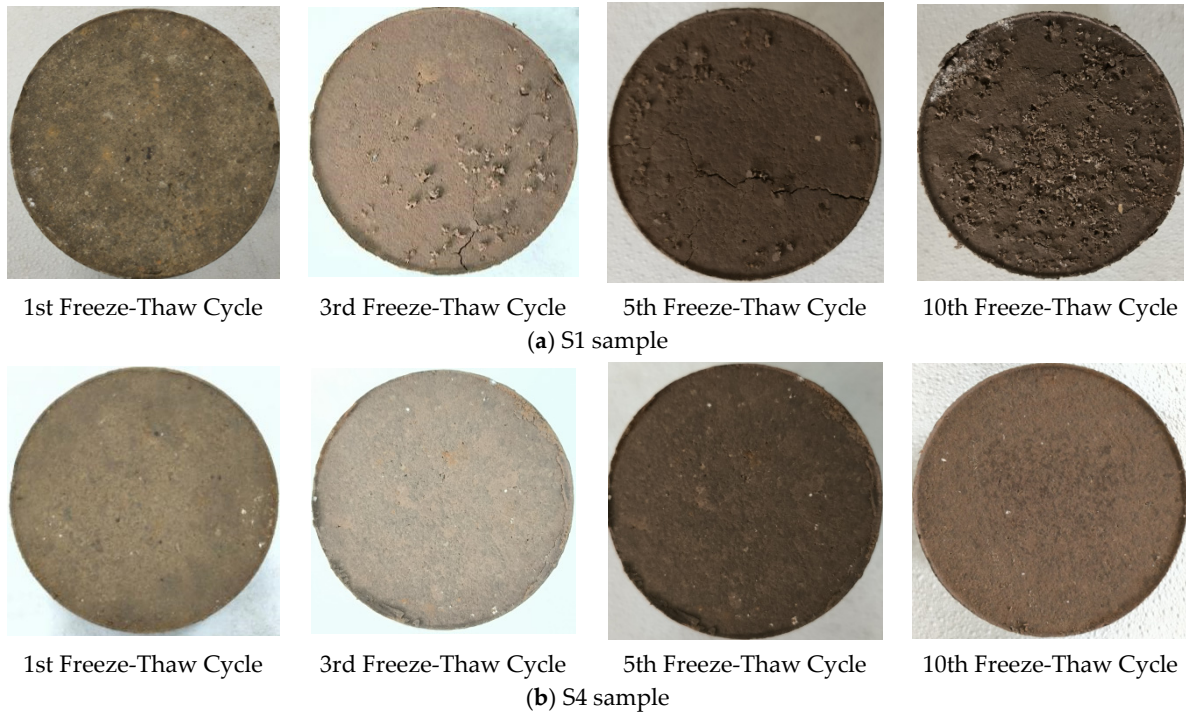


Figure 10. Surface changes of S1 sample and S4 sample under freeze-thaw conditions.

From Figures 11 and 12, it can be seen that after 10 freeze-thaw cycles, the UCS of S2–S5 was 1.04 MPa, 1.28 MPa, 2.01 MPa, and 1.89 MPa, respectively, significantly higher than that of S1 (i.e., 0.3 MPa). The UCS losses of samples S2–S5 were 23.4%, 21.8%, 19.3%, and 25.3%, respectively, significantly lower than that of S1 (i.e., 59.6% MPa). These indicate that the addition of lignin and BFS can improve the soil's freeze-thaw resistance.

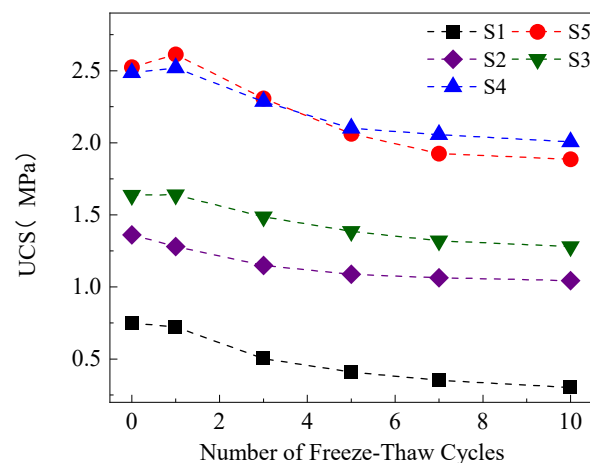
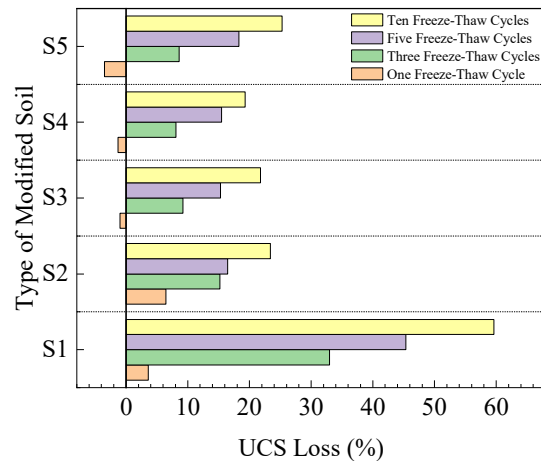


Figure 11. The relationship between the number of freeze-thaw cycles and the UCS.





**Figure 12.** Strength loss values after freeze-thaw cycles.

In addition, the samples doped with BFS (i.e., S3–S5) showed strength enhancement after the first freeze-thaw cycle. The reason for this is that, during the freezing process, the micro-cracks formed by frost heave in the soil accelerated the water diffusion, which promoted the hydration reaction of BFS. The gelled material generated by hydration filled the micro-cracks and particle pores and restored or even enhanced the strength of the soil to a certain extent. However, with the increase in the number of freeze-thaw cycles, this effect gradually weakened and eventually disappeared.

### 3.4. Correlation Analysis

To further clarify the effects of lignin and BFS content on the mechanical and freeze-thaw properties of silty clay, the linear regression method was used to analyze the growth rate of UCS after 28 days of curing and the loss rate of UCS after freeze-thaw cycles [52]. The interaction between the two factors is shown in Figures 13 and 14. With the increase in lignin and BFS content, the response surface curve of UCS growth rate showed a trend of first increasing and then decreasing, and the response surface curve of the UCS loss rate during the freeze-thaw cycle showed a trend of first decreasing and then increasing, indicating that there was an optimal proportion of lignin and BFS content. Through linear regression, under the condition of an improver dosage of 12%, the UCS growth rate was the largest when lignin: BFS = 4.17%:7.93%, and the UCS loss rate after freezing and thawing was the smallest when lignin: BFS = 4.128%:7.972%. The above results are close to the ratio of modifiers in the S4 sample. Therefore, when lignin: BFS  $\approx$  4%:8%, the soil improvement effect is most significant and the freeze-thaw resistance is the highest.

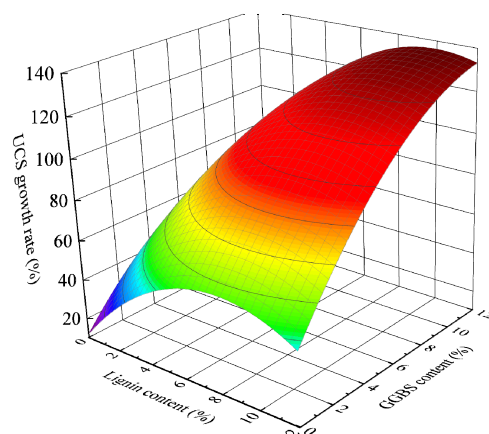


**Figure 13.** Response surface of the unconfined compressive strength growth rate.

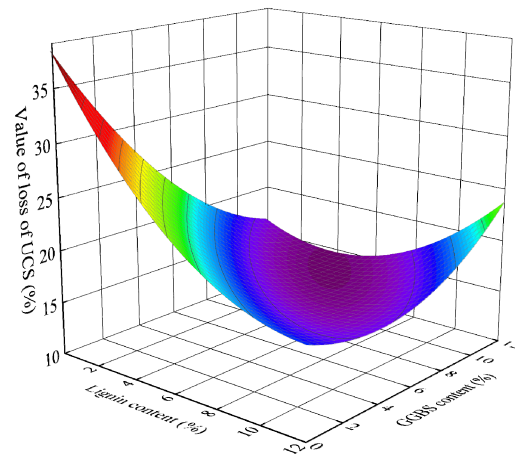


Figure 14. Response surface of the rate of UCS loss for the 10th freeze-thaw cycle.

### 3.5. Microscopic Analysis

#### 3.5.1. SEM Analysis

Using SEM, MIP, and  $^1\text{H}$  NMR, the optimization effect of the modifier (lignin and blast furnace slag) on the microstructure of silty clay was investigated. The samples were the unmodified sample (S1) and the best modified sample (S4), and the samples underwent different freeze-thaw cycles (0, 5, 10). Figure 15b,d shows the morphologies of the S1 and S4 samples under 1000-magnification electron microscope scanning after curing for 28 days. The mercury intrusion volume under different pressures was recorded using a mercury injection meter. Figure 16 shows the pore size distribution curve. Compared with the S1 sample and the S4 sample, the pore size distribution of the modified sample (S4) was more concentrated in the range of middle and small holes, indicating optimized pore distribution. In the  $^1\text{H}$  NMR test, samples with a saturated water state were prepared and put into a nuclear magnetic resonance instrument to measure the relaxation time distribution. Figure 17 shows that, in the S4 sample, the proportion of water in small pores increased, indicating better water retention performance and pore stability.

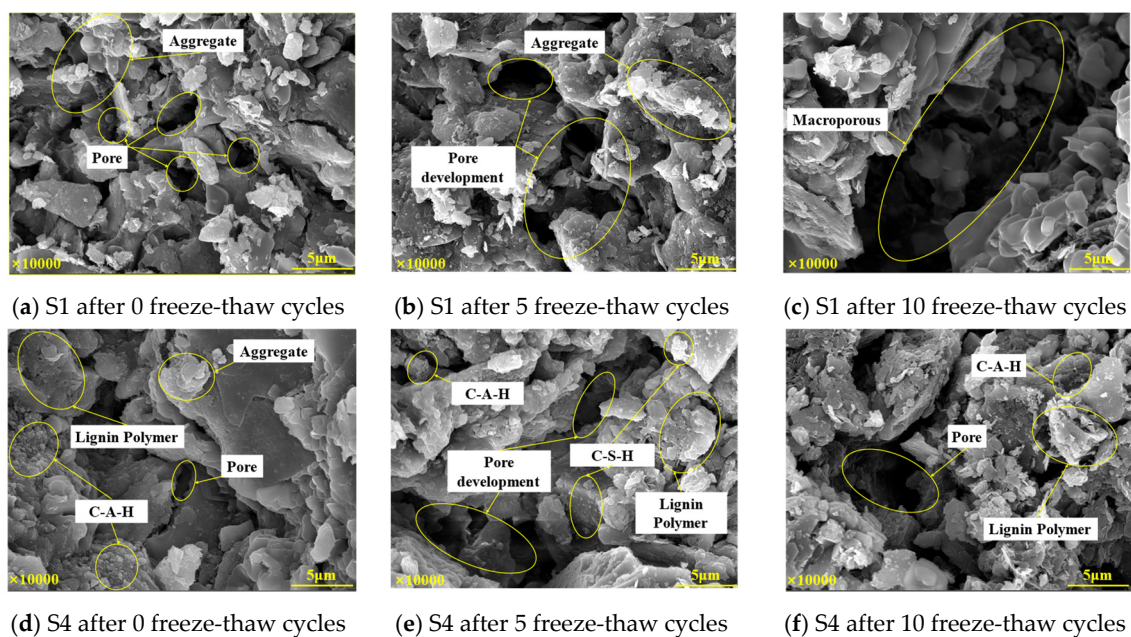


Figure 15. Microscopic appearance of the S1 sample and the S1 sample.

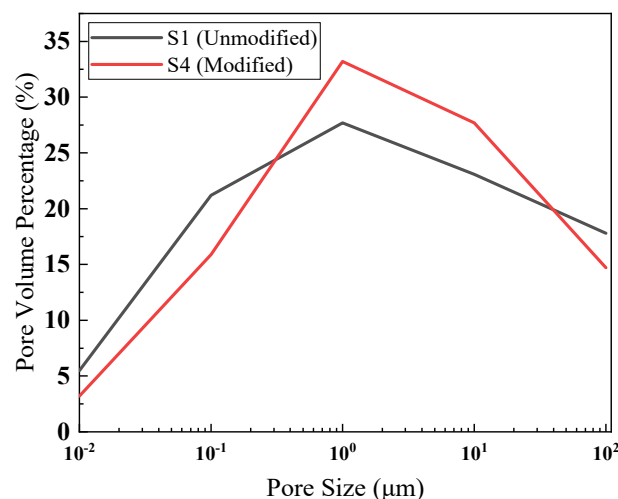


Figure 16. Pore Size Distribution (MIP).

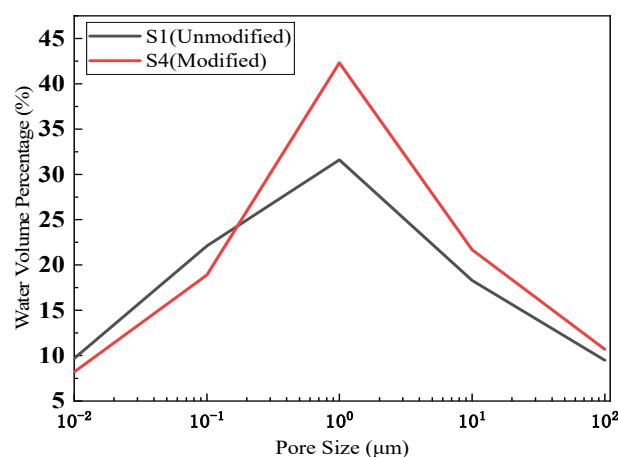


Figure 17. Pore Water Distribution (1H NMR).

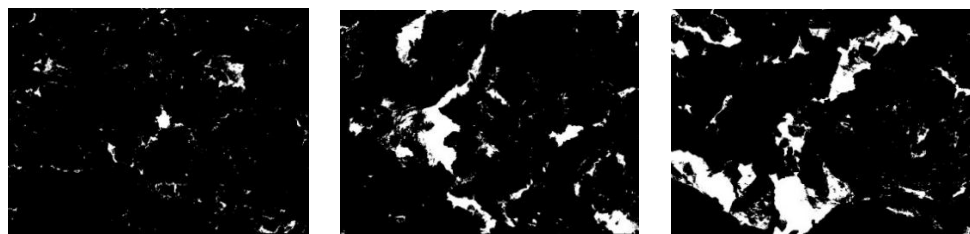
Calcium silicate hydrate (C-S-H) and calcium aluminate hydrate (C-A-H) produced by BFS hydration exist mainly in the form of flocculation, accumulating between soil particles and on the surface to fill gaps and support bones. As can be seen from Figure 15a, the particle surface of the S1 sample is smooth, the boundary is clear, and the skeleton unit is mainly connected by contact. There is an obvious pore structure between the particles and the lack of cementing material, which indicates that the microstructure of the unmodified sample is loose and the compressive strength is low. As can be seen from Figure 15d, after adding lignin and BFS, the structural characteristics of the S4 sample have changed significantly; the cementing material has increased significantly, small debris particles and amorphous substances bind to each other to cover the debris particles, and a large number of flocculating and cementing substances are filled between the particles. The SEM images (Figure 15) reveal typical C-S-H morphologies, appearing as gel-like and flocculent substances that fill soil pores and form strong inter-particle bridges. These hydration products not only enhance the bonding between particles but also significantly reduce porosity, resulting in a denser and more cohesive soil structure. No similar structure was observed in the unmodified sample (S1), further demonstrating the significant effect of the modifier. The formation of hydration products was verified in terms of microstructure and phase changes. The positively charged polymer formed by the protonation of lignin wraps the fine detritus particles into clumps and attaches to the structural skeleton units, increases the base-base bond and strength of the structural skeleton, and reduces the number and size of pores.

As seen in Figure 15b,e, after five freeze-thaw cycles, the original surface-to-surface contact aggregate structure of the S1 sample gradually breaks down, and the clay minerals shift from a directional structure to a disordered structure. The effect of the bonding structure between particles in the S4 sample was weakened, the soil particles wrapped by the gelled products were gradually eroded, and the bonding efficiency of the gelled products was destroyed. The aggregate skeleton structure was gradually loosened, the surface particles fell off, and small pores appeared. From Figure 15c,f, after ten freeze-thaw cycles, cracks and large holes appeared inside the S1 sample, and the integrity of the soil was damaged. In the S4 sample, some aggregate particles were damaged, small pores and cracks increased, and no cracks appeared, so the sample was relatively complete. In general, compared to the S1 sample, the S4 sample exhibits better overall integrity and tighter agglomeration after freeze-thaw cycles. Under the action of the cementation of hydration products and skeleton construction, the soil structure of the S4 sample remains uniform and dense, which prevents the continuous damage of the soil microstructure caused by the freeze-thaw cycle. Therefore, the modified soil samples show strong structural stability and damage resistance under the action of the freeze-thaw cycle, and the integrity and density are significantly better than the undisturbed soil.

To further analyze the pore changes under freeze-thaw cycles, image recognition technology was used to binarize the SEM images [53]. The processing results are shown in Figure 18, where the black part represents particles and the white part represents pores. According to Figure 18, the pore ratio (the ratio of the pore area to the total area) of the S1 and S4 samples for different freeze-thaw cycles was calculated, as shown in Figure 19. In order to reduce the error caused by SEM, a wider sampling strategy was adopted. In the sample preparation process, multiple slices were cut from different positions (such as the center, edge, top, bottom, etc.), different directions (horizontal, vertical, etc.), and different magnifications of SEM for observation, using professional image analysis software 1.8.0 to process SEM images.



(a) S1 after 0 freeze-thaw cycles (b) S1 after 5 freeze-thaw cycles (c) S1 after 10 freeze-thaw cycles



(d) S4 after 0 freeze-thaw cycles (e) S4 after 5 freeze-thaw cycles (f) S4 after 10 freeze-thaw cycles

**Figure 18.** Result of binarization of the image.

From Figure 19, it can be seen that as the number of freeze-thaw cycles increases, the porosity of the sample gradually increases, and the porosity of sample S4 is significantly reduced compared to sample S1, indicating that the addition of lignin and BFS can effectively reduce the porosity of the sample. To analyze the correlation between the mechanical properties of soil and the degree of pore damage, a Cartesian coordinate

system was established between the total pore area and macroscopic mechanical strength parameters. The mathematical relationship between the two was fitted and analyzed, and the correlation coefficient exceeded 0.92; the results are shown in Figure 20. As the total pore area increases, the UCS of samples S1 and S4 gradually decreases, indicating that freeze-thaw action disrupts the arrangement and contact of soil particles, increases the porosity and pore area, weakens the bonding force between the particles, and results in the looseness of soil structure and the decrease in soil strength. In the same pore area, the UCS strength of the S4 sample is much higher than that of the S1 sample, indicating that lignin and BFS have a significant effect on improving the mechanical properties of silty clay.

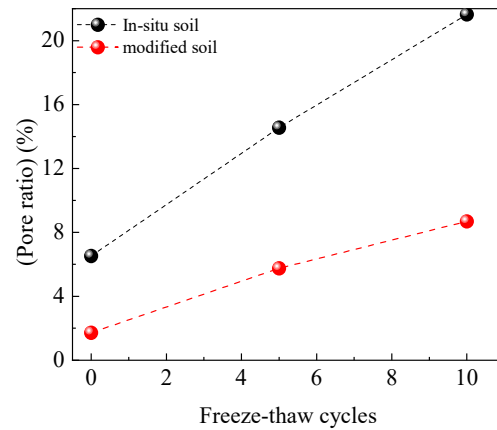


Figure 19. The relationship curve between porosity and the number of freeze-thaw cycles.

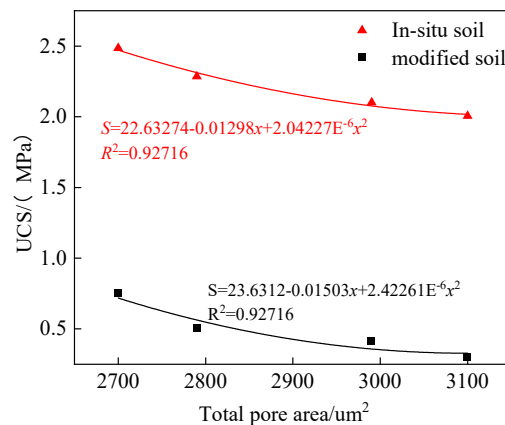


Figure 20. Relationship between macro mechanical parameters and total pore area.

### 3.5.2. X-Ray Diffraction

The selection of the S1 sample after curing for 7 days and the S4 sample after curing for 7 days and 28 days for the XRD study was mainly based on the following reasons. For the control group without added lignin and BFS (BFS), the XRD results of sample S1 show the mineral composition of the original soil, providing a basis for subsequent comparison. The S4 sample has shown good performance in previous tests of unconfined compressive strength, CBR, the resilience modulus, the freeze-thaw cycle, etc. It can be selected to explore changes in soil mineral composition after different curing times under the action of this specific ratio of lignin and BFS, so as to further understand the influence mechanism of the modifier on the soil mineral structure. The comparison of the S4 samples with a curing time of 7 days and 28 days is helpful to study the chemical reaction and mineral transformation process of the modified system over time and to explain its influence on the long-term soil properties from the microscopic level. This is closely related to the whole



study of lignin-BFS-modified silty clay and can complement other test results, making the research more comprehensive and systematic.

Sample S1, which was cured for 7 days, and sample S4, which was cured for 7 days and 28 days, were selected for XRD analysis. The main mineral composition of each group is shown in Figure 21. After 7 days of solidification, the main diffraction peaks of the S1 and S4 samples are similar, and the main components are quartz and kaolinite, followed by nano-feldspar. The diffraction peaks of the S4 samples at  $26^\circ$  and  $33^\circ$  are significantly enhanced, representing the amorphous C-S-H characteristic signals. These peaks indicate the hydration reaction of BFS in an alkaline environment, where silicate ( $\text{SiO}_4^{4-}$ ) and calcium ions ( $\text{Ca}^{2+}$ ) form an amorphous gel-like structure. This reaction is further supported by weak peaks corresponding to C-A-H (ettringite), highlighting the presence of secondary hydration products. The peak strength of the S4 sample was significantly enhanced at these locations compared to the S1 sample, further demonstrating an increase in hydration products. The results showed that the hydration reaction produced remarkable C-S-H products during the modification of BFS. The results were further verified by SEM images. The particles of S4 are flocculent and gel-like, demonstrating a typical C-S-H structure, filling the soil pores and forming a bridge between the particles. In contrast, no similar structure (S1) was observed in the unmodified samples, further demonstrating the important role of the modifier. Combined with SEM and PXRD, it can be confirmed that C-S-H and C-A-H hydration products are significantly generated after BFS modification. The flocculation and gelling properties of C-S-H significantly improved the strength and stability of the soil by filling the pores and strengthening the particle connection, while the protonation of lignin enhanced the electrostatic adsorption effect between the particles and further optimized the microscopic skeleton structure of the soil. After curing for 28 d, the diffraction peak of the hydrated products increased slightly, indicating that more C-S-H, C-A-H, and other crystal structures were produced with the extension of curing time, further indicating that the existence and content of hydrated calcium silicate changed with the change of the curing process.

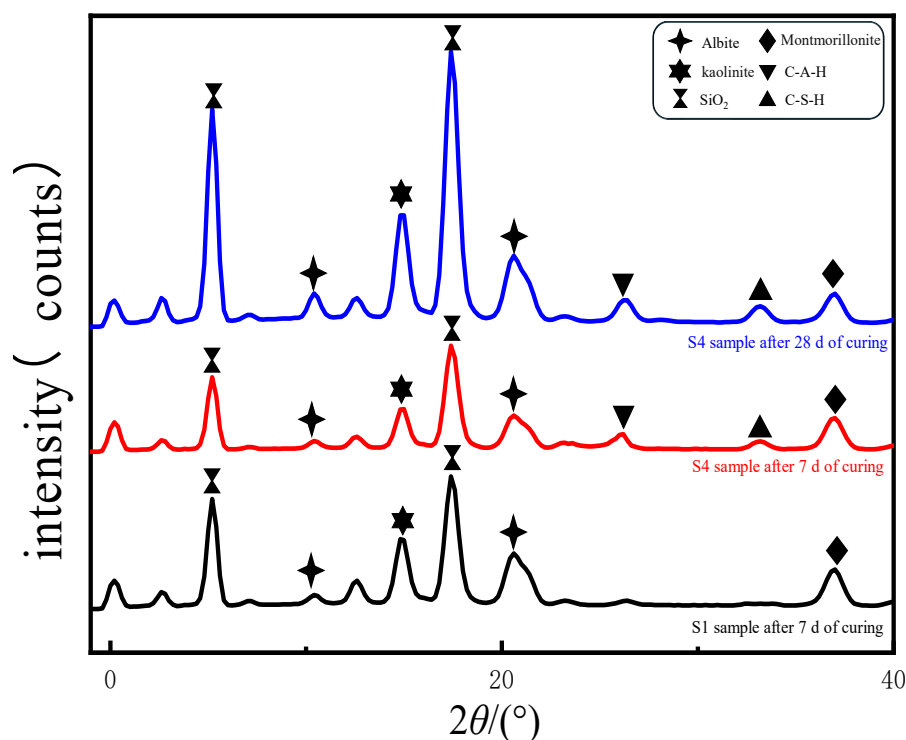


Figure 21. X-ray diffraction pattern.

### 3.6. Modification Mechanism

According to the results of the SEM test and XRD, the mechanism of lignin-BFS-modified silty clay mainly includes a protonation reaction, a hydration reaction, and an ion reaction. Under the action of electrostatic attraction, the positively charged lignin polymer attracts the negatively charged clay minerals to form covalent bonds and finally forms cementation at the contact point, which plays a role in strengthening the soil. The hydration of dicalcium silicate (C2S), tricalcium silicate (C3S), and tricalcium aluminate (C3A) in BFS produces C-S-H and C-A-H, which play critical roles in enhancing soil strength. The XRD results (Figure 21) confirm the formation of C-S-H through the enhanced diffraction peaks at  $26^\circ$  and  $33^\circ$ . These products fill soil pores and create a three-dimensional network structure that binds soil particles together. SEM images (Figure 15) further show gel-like and flocculent structures, which are typical morphologies of C-S-H, improving the soil's mechanical properties.

As seen in Figure 22, FTIR technology can detect the vibration absorption of molecules to analyze the changes of chemical bonds and functional groups, which is of great significance to study the mechanism of lignin-BFS-modified silty clay. The absorption peak of lignin functional groups changed before and after modification. Before modification, the stretching vibration peak of the lignin alcohol hydroxyl group (-OH) was around  $3374\text{ cm}^{-1}$ . After modification, if the functional groups involved in the reaction, such as hydroxyl, to form hydrogen bonds, the relevant peak position, strength, benzene ring C=C bond, alkane (C-H ( $\text{CH}_2$ )), primary alcohol ( $\text{R}_1\text{-CH}_2\text{-OH}$ ) and secondary alcohol ( $\text{R}_1\text{-CH(R}_2\text{)-OH}$ ), and other functional group peaks will also change accordingly. The interaction with BFS and clay was reflected. BFS hydration products have characteristic peaks in FTIR, which can be used to determine the degree of hydration reaction and the products and to understand its role in strengthening soil strength. FTIR is combined with XRD and SEM. XRD provides crystal structure information, FTIR supplements chemical bond analysis and explains the reasons for structural changes, and SEM displays the microscopic morphology to jointly build a complete understanding of the modification mechanism.

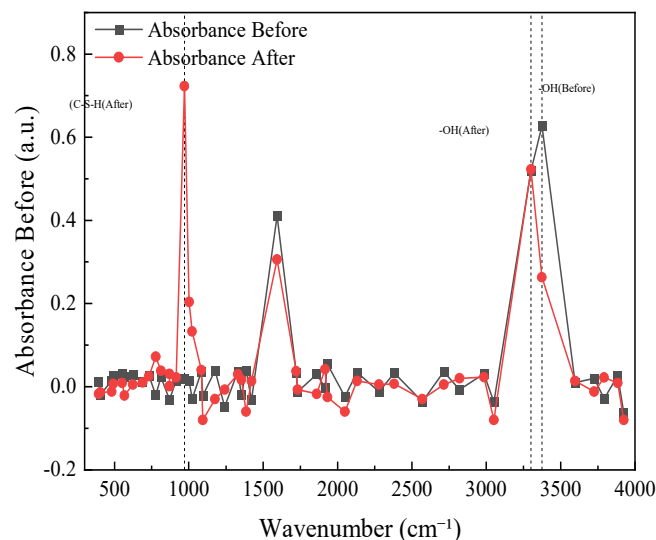
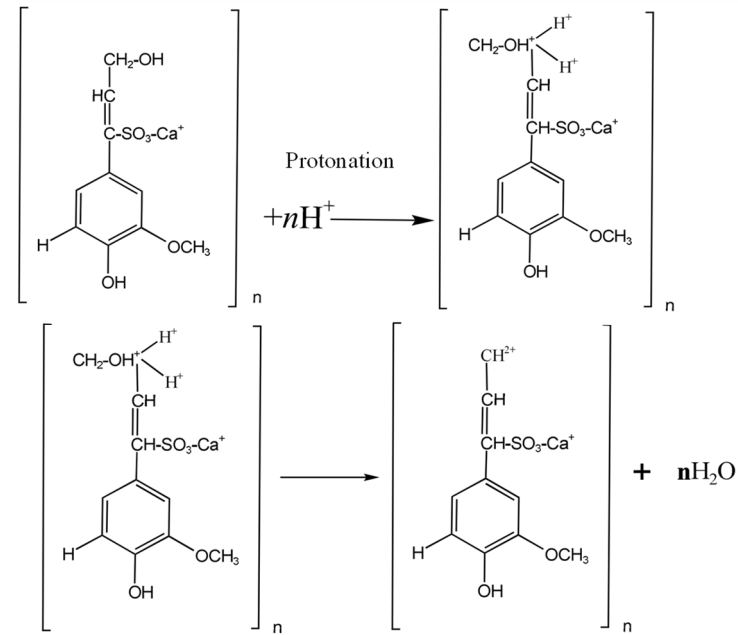


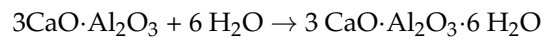
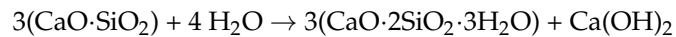
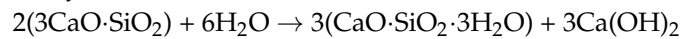
Figure 22. FTIR Spectra of Modified and Unmodified Silty Clay.

The chemical reaction equation is as follows:

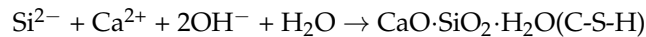
## (1) protonation



## (2) hydration reaction



## (3) ionic reaction



## 4. Conclusions

In this paper, the mechanics, road performance, and freeze-thaw properties of lignin-BFS-modified silty clay were studied, and the optimal dosage of lignin and BFS was determined. The modification mechanism was analyzed using SEM and XRD tests. The main conclusions are as follows:

- (1) The mechanical properties of modified soil significantly improved. The CBR and rebound modulus of the modified soil meet the standard requirements of the roadbed and pavement. As the curing age increases, the UCS of modified soil gradually increases, the failure strain gradually decreases, and the stress-strain curve transitions from strain-softening to strain-hardening. The UCS, CBR, and rebound modulus all show a trend of first increasing and then stabilizing with the decrease in lignin content and the increase in BFS content.
- (2) As the number of freeze-thaw cycles increases, the number of fine micro-cracks and large pores in the soil increases, the density between soil particles decreases, and the phenomenon of soil particle detachment appears on the surface, the mass loss rate and volume expansion rate of soil samples gradually increases and the strength decreases. The addition of lignin and BFS can effectively limit the generation of large pores and the expansion of cracks, resist mass loss and volume increase caused by freeze-thaw cycles, effectively alleviate the damage of freeze-thaw cycles to soil strength, and improve soil strength.
- (3) Based on indoor experiments and linear regression analysis, there is an optimal ratio between lignin and BFS. When the ratio of the two is 4%: 8%, the growth rate of UCS, the CBR value, and the rebound modulus of modified soil are the highest, and the

volume and mass changes and compressive strength loss under freeze-thaw cycles are the smallest. The soil improvement effect is the most significant.

- (4) According to the SEM test results and XRD analysis, the addition of lignin and BFS in the silty clay mainly produces a protonation reaction, a hydration reaction, and an ion reaction. The generated products and structures work together to improve the strength of the soil skeleton, reduce porosity, and enhance the bonding and cohesion between particles.

**Author Contributions:** Y.S.: Writing—review and editing, Supervision, Conceptualization. F.Y.: Methodology, Writing—review and editing. Y.Y.: Writing—review and editing, Funding acquisition. C.L.: Investigation, Data curation. S.X.: Writing—original draft, Funding acquisition. J.H.: Investigation. All authors have read and agreed to the published version of the manuscript.

**Funding:** The authors gratefully acknowledge the National Natural Science Foundation of China by Yang Yu (Grant no. 51774167), Xinjiang Tianchi Talent Introduction Program (Grant No. 2024XGYT-CYC01), and the Lianyungang Science and Technology Plan Project (Grant no. ICY2315).

**Data Availability Statement:** Data will be made available on request.

**Conflicts of Interest:** The authors declare no conflicts of interest.

## References

1. Qiu, E.; He, Q.; Chen, Q.; Sun, X.; Zhang, R.; Qu, M.; Wan, X. Influence of freeze-thaw cycles on mechanical properties of moraine soils. *Transp. Geotech.* **2023**, *42*, 101097. [[CrossRef](#)]
2. Lu, Z.; Xian, S.; Yao, H.; Fang, R.; She, J. Influence of freeze-thaw cycles in the presence of a supplementary water supply on mechanical properties of compacted soil. *Cold Reg. Sci. Technol.* **2019**, *157*, 42–52. [[CrossRef](#)]
3. Chen, H.; Gao, X.; Wang, Q. Research progress and prospect of frozen soil engineering disasters. *Cold Reg. Sci. Technol.* **2023**, *212*, 103901. [[CrossRef](#)]
4. Li, H. Several harmful geological phenomena of weak rock slope in subgrade engineering and prevention measures. *Chin. J. Rock Mech. Eng.* **2002**, *21*, 1404–1407.
5. Yuan, B.; Li, Z.; Chen, Y.; Ni, H.; Zhao, Z.; Chen, W.; Zhao, J. Mechanical and microstructural properties of recycling granite residual soil reinforced with glass fiber and liquid-modified polyvinyl alcohol polymer. *Chemosphere* **2022**, *286*, 131652. [[CrossRef](#)]
6. Zornberg, J.G. Functions and Applications of Geosynthetics in Roadways. *Procedia Eng.* **2017**, *189*, 298–306. [[CrossRef](#)]
7. Liu, Z.; Cai, C.S.; Liu, F.; Fan, F. Feasibility Study of Loess Stabilization with Fly Ash-Based Geopolymer. *J. Mater. Civ. Eng.* **2016**, *28*, 4016003. [[CrossRef](#)]
8. Ullah, A.; Boumezerane, D.; Ahmad, F. Subgrade improvement with mixed lime and cement as additives. *Mater. Today Proc.* **2023**; *in press*. [[CrossRef](#)]
9. Jia, L.; Guo, J.; Wei, Z.; Wu, R. Mix optimization and mechanical properties evaluation of lime-fly ash-stabilized loess in various engineering applications. *Case Stud. Constr. Mater.* **2024**, *20*, e03208. [[CrossRef](#)]
10. Eyo, E.U.; Ng’Ambi, S.; Abbey, S.J. Incorporation of a nanotechnology-based additive in cementitious products for clay stabilization. *J. Rock Mech. Geotech. Eng.* **2020**, *12*, 1056–1069. [[CrossRef](#)]
11. Abbey, S.J.; Ngambi, S.; Ganjian, E. Development of Strength Models for Prediction of Unconfined Compressive Strength of Cement/Byproduct Material Improved Soils. *Geotech. Test. J.* **2017**, *40*, 928–935. [[CrossRef](#)]
12. Zhang, B.; Jiang, W.; Xu, Q.; Yuan, D.; Shan, J.; Lu, R. Experimental feasibility study of ethylene-vinyl acetate copolymer (EVA) as cement stabilized soil curing agent. *Road Mater. Pavement Des.* **2022**, *23*, 617–638. [[CrossRef](#)]
13. Onyelowe, K.C. Review on the role of solid waste materials in soft soils reengineering. *Mater. Sci. Energy Technol.* **2019**, *2*, 46–51. [[CrossRef](#)]
14. Amakye, S.Y.; Abbey, S.J.; Booth, C.A.; Mahamadu, A.-M. Enhancing the Engineering Properties of Subgrade Materials Using Processed Waste: A Review. *Geotechnics* **2021**, *1*, 15. [[CrossRef](#)]
15. Yu, J.; Vaidya, M.; Su, G.; Adhikari, S.; Korolev, E.; Shekhovtsova, S. Experimental study of soda lignin powder as an asphalt modifier for a sustainable pavement material. *Constr. Build. Mater.* **2021**, *298*, 123884. [[CrossRef](#)]
16. Moretti, C.; Corona, B.; Hoefnagels, R.; Vural-Gürsel, I.; Gosselink, R.; Junginger, M. Review of life cycle assessments of lignin and derived products: Lessons learned. *Sci. Total Environ.* **2021**, *770*, 144656. [[CrossRef](#)]
17. Chio, C.; Sain, M.; Qin, W. Lignin utilization: A review of lignin depolymerization from various aspects. *Renew. Sustain. Energy Rev.* **2019**, *107*, 232–249. [[CrossRef](#)]

18. Matcha, B.; Sudhir, M.R.; Chen, S.; Rai, S.; Jain, D. An Empirical Model for Geopolymer Reactions Involving Fly Ash and GGBS. *Adv. Mater. Sci. Eng.* **2022**, *2022*, 8801294.
19. Torres, L.A.Z.; Woiciechowski, A.L.; de Andrade Tanobe, V.O.; Karp, S.G.; Lorenci, L.C.G.; Faulds, C.; Soccol, C.R. Lignin as a potential source of high-added value compounds: A review. *J. Clean. Prod.* **2020**, *263*, 121499. [[CrossRef](#)]
20. Bajwa, D.S.; Pourhashem, G.; Ullah, A.H.; Bajwa, S.G. A concise review of current lignin production, applications, products and their environmental impact. *Ind. Crops Prod.* **2019**, *139*, 111526. [[CrossRef](#)]
21. Sargent, P.; Hughes, P.N.; Rouainia, M. A new low carbon cementitious binder for stabilising weak ground conditions through deep soil mixing. *Soils Found.* **2016**, *56*, 1021–1034. [[CrossRef](#)]
22. Hou, X.; Ma, W.; Li, G.; Mu, Y.; Zhou, Z.; Wang, F. Influence of lignosulfonate on mechanical properties of Lanzhou loess. *Rock Soil Mech.* **2017**, *38* (Suppl. S2), 18–26. [[CrossRef](#)]
23. Zhang, J.; Qian, S.; Wang, X.; Bian, H.; Han, Z.; Shi, L. Experimental study on resistance of EICP and lignin joint-modified silt slope to rain erosion. *J. Hohai Univ. (Nat. Sci.)* **2024**, *52*, 70–76.
24. Dong, C.; Huang, Y.; Zhang, W.; Tang, X.; Gu, Y.; Feng, Y. Behavioral evaluation on the engineering properties of lignin-stabilized loess: Reuse of renewable materials. *Constr. Build. Mater.* **2023**, *369*, 130599. [[CrossRef](#)]
25. Zhang, H.; Lin, C.; Sheng, Y. Experimental study of engineering properties of loess reinforced by consolid system. *Yanshilixue Yu Gongcheng Xuebao/Chin. J. Rock Mech. Eng.* **2015**, *34*, 3574–3580. [[CrossRef](#)]
26. Zhang, T.; Liu, S.; Zhan, H.; Ma, C.; Cai, G. Durability of silty soil stabilized with recycled lignin for sustainable engineering materials. *J. Clean. Prod.* **2020**, *248*, 119293. [[CrossRef](#)]
27. Liu, Y.; Cao, C.; Wang, Q.; Zheng, W.; Shen, J.; Chen, Y.; Gu, F.; Han, M.; Rocchi, I. Utilization of bioethanol industry recycled waste for sustainable soil improvement: A win-win application. *Eng. Geol.* **2021**, *289*, 106192. [[CrossRef](#)]
28. Zhu, F.; Li, J.; Jiang, W.; Zhang, S.; Dong, W. Freeze-Thaw Performance of Silt Sand Treated with Lignin. *Adv. Civ. Eng.* **2021**, *2021*, 6639268. [[CrossRef](#)]
29. Alazigha, D.P.; Indraratna, B.; Vinod, J.S.; Heitor, A. Mechanisms of stabilization of expansive soil with lignosulfonate admixture. *Transp. Geotech.* **2018**, *14*, 81–92. [[CrossRef](#)]
30. Preetham, H.K.; Nayak, S. Geotechnical Investigations on Marine Clay Stabilized Using Granulated BFS and Cement. *Int. J. Geosynth. Ground Eng.* **2019**, *5*, 28. [[CrossRef](#)]
31. Li, L.H.; Li, X.; Li, W.T.; Zhou, X.L. Mechanical and leaching characteristics of copper-contaminated soil solidified by soda residue-sla. *China Sci.* **2023**, *18*, 687–693.
32. Li, L.; Li, Z.; Xiao, H.; Huang, S.; Liu, Y. Engineering characteristics and mechanism of rice husk ash-ground granulated blast slag cured expansive soil. *J. Zhejiang Univ. (Eng. Sci.)* **2023**, *57*, 1736–1745. [[CrossRef](#)]
33. Zhu, M.; Xie, G.; Liu, L.; Wang, R.; Ruan, S.; Yang, P.; Fang, Z. Strengthening mechanism of granulated blast-furnace slag on the uniaxial compressive strength of modified magnesium slag-based cemented backfilling material. *Process Saf. Environ. Prot.* **2023**, *174*, 722–733. [[CrossRef](#)]
34. Mujtaba, H.; Aziz, T.; Farooq, K.; Sivakugan, N.; Das, B.M. Improvement in Engineering Properties of Expansive Soils using Ground Granulated BFS. *J. Geol. Soc. India* **2018**, *92*, 357–362. [[CrossRef](#)]
35. Devarangadi, M.; Vuppala, S.; Shankar, M.U.; Raghunandan, M.E. Effect of collated fly ash, GGBS and silica fume on index and engineering properties of expansive clays as a sustainable landfill liner. *Clean. Mater.* **2024**, *11*, 100219. [[CrossRef](#)]
36. Corrêa-Silva, M.; Miranda, T.; Rouainia, M.; Araújo, N.; Glendinning, S.; Cristelo, N. Geomechanical behaviour of a soft soil stabilised with alkali-activated blast-furnace slags. *J. Clean. Prod.* **2020**, *267*, 122017. [[CrossRef](#)]
37. Gupta, S.; Kumar, S. Mechanical and microstructural analysis of soft kaolin clay stabilized by GGBS and dolomite-based geopolymer. *Constr. Build. Mater.* **2024**, *421*, 135702. [[CrossRef](#)]
38. Parhizkar, A.; Nazarpour, A.; Khayat, N. Investigation of geotechnical and microstructure characteristics of gypsum soil using ground granulated blast-furnace slag (GGBS), fly ash, and lime. *Constr. Build. Mater.* **2024**, *418*, 135358. [[CrossRef](#)]
39. Chai, S.; Zhang, L. Study on damage mechanism of alkali activated fly ash mineral powder modified expansive soil under drying wetting freezing thawing cycles. *Eng. Mech.* **2024**, *41*, 157–167. [[CrossRef](#)]
40. Zhu, X.; Niu, F.; Ren, L. Novel selection of environment-friendly curing agents for thawing permafrost: Alkali-activated ground granulated blast-furnace slag. *Cold Reg. Sci. Technol.* **2023**, *211*, 103863. [[CrossRef](#)]
41. Zhang, Y.; Liu, W.; Liu, M. Setting time and mechanical properties of chemical admixtures modified FA/GGBS-based engineered geopolymer composites. *Constr. Build. Mater.* **2024**, *431*, 136473. [[CrossRef](#)]
42. Qi, W.; Duan, G.; Han, Y.; Zhao, Q.; Huang, Y.; Zhu, W.; Pang, H.; Zhang, J. Comparison of mechanical properties and microstructure of GGBS-based cementitious materials activated by different combined alkaline wastes. *Constr. Build. Mater.* **2024**, *422*, 135784. [[CrossRef](#)]
43. Kim, M.J.; Ishida, T.; Cho, W.J. Characteristics of micro structure and strength development of alkali activated GGBS-FNS hybrid cement. *Constr. Build. Mater.* **2023**, *408*, 133773. [[CrossRef](#)]



44. Li, H.; Wang, R.; Wei, M.; Lei, N.; Wei, T.; Liu, F. Characteristics of carbide-slag-activated GGBS–fly ash materials: Strength, hydration mechanism, microstructure, and sustainability. *Constr. Build. Mater.* **2024**, *422*, 135796. [[CrossRef](#)]
45. Liu, Z.; Wang, Q.; Zhong, X.; Liu, F. Water holding capacity and water stability of lignin-modified loess. *Chin. J. Rock Mech. Eng.* **2020**, *39*, 2582–2592. [[CrossRef](#)]
46. Zhang, J.; Wang, X.; Li, B.; Han, Y.; Bian, H. Experimental study on silt reinforced by EICP-lignin technology. *J. Civ. Environ. Eng.* **2021**, *43*, 201–202.
47. *JTG 3430-2020; Test Methods of Soils for Highway Engineering*. Ministry of Transport: Beijing, China, 2020.
48. Yang, X.; Fang, Y.; Liu, J.; Zhang, X.; Yue, Y. Mechanical Properties and Microscopic Mechanism of Rice Husk Ash-Cement Improved Mucky Soft Soils. *Soil Eng. Found.* **2022**, *36*, 977–979. Available online: <http://tgj.whrsm.ac.cn/EN/Y2022/V36/I6/977> (accessed on 23 December 2024).
49. Nagaraj, H.B.; Suresh, M.R. Influence of clay mineralogy on the relationship of CBR of fine-grained soils with their index and engineering properties. *Transp. Geotech.* **2018**, *15*, 29–38. [[CrossRef](#)]
50. *JTG D50-2017; Specifications for Design of Highway Asphalt Pavement*. Ministry of Transport: Beijing, China, 2017.
51. Zhao, X.; Shen, Z.; Deng, Y.; Li, J.; Yue, Z.; Liang, T. Freeze-thaw Resistance and Deterioration Mechanism of Cement-treated Mixture of Soda Residue and Clay. *China J. Highw. Transp* **2024**, *37*, 55–65. [[CrossRef](#)]
52. Zhang, Q.-Q.; Lu, Y.; Li, Z.-B.; Cui, W.; Lei, M.-Q.; Wang, S.-J. Study on performance and application of O-QGS soil curing agent for waste clay with low liquid limit. *Constr. Build. Mater.* **2024**, *436*, 136986. [[CrossRef](#)]
53. Jiang, M.; Wu, D.; Cao, P.; Ding, Z. Connected inner pore analysis of calcareous sands using SEM. *Chin. J. Geotech. Eng.* **2017**, *39* (Suppl. S1), 1–5. [[CrossRef](#)]

**Disclaimer/Publisher’s Note:** The statements, opinions and data contained in all publications are solely those of the individual author(s) and contributor(s) and not of MDPI and/or the editor(s). MDPI and/or the editor(s) disclaim responsibility for any injury to people or property resulting from any ideas, methods, instructions or products referred to in the content.